IOP Conf. Series: Journal of Physics: Conf. Series **840** (2017) 012028 doi:10.1088/1742-6596/840/1/012028

MICROSCOPE: five months after launch

Joel Bergé[1], Pierre Touboul[1], Manuel Rodrigues[1], Françoise Liorzou[1]

[1] ONERA, the French Aerospace Lab, 29 avenue de la Division Leclerc, 92320 Châtillon, France

E-mail: joel.berge@onera.fr

Abstract. MICROSCOPE is a French Space Agency mission that aims to test the Weak Equivalence Principle in space down to an accuracy of 10^{-15}, two orders of magnitude better than the current constraints. The MICROSCOPE satellite was launched on April 25, 2016. We describe the MICROSCOPE mission, its measurement principle and instrument, and report on the status of its in-orbit commissioning as of September 2016.

1. Introduction

From the deviation of Mercury's perihelion to gravitational redshift to gravitational waves to the existence of black holes, General Relativity (GR) continues to pass experimental tests one century after its inception. The recent direct detection of gravitational waves by LIGO [1, 2] not only superbly matches expectations from GR, but it also directly proves the existence of back holes. So many successes would tend to consider GR as the correct theory for gravitation. However, fundamental physics has faced major challenges for decades: how to unify the (as successful) quantum standard model of particle physics with GR, and how to explain the acceleration of the cosmological expansion?

To answer those questions, we may need to look deeply in the foundations of GR themselves. A particularly important test is to look for a violation of the Weak Equivalence Principle (WEP), a cornerstone of GR. MICROSCOPE (Micro-Satellite à traînée Compensée pour l'Observation du Principe d'Equivalence [3, 4, 5]) is a drag-free microsatellite which aims to test the WEP down to the 10^{-15} level, and was launched on April 25, 2016. In this paper, we first briefly introduce the WEP in Sect. 2; we then give a short overview of MICROSCOPE in Sect. 3 before stating on its status (as of September 2016) in Sect. 4. We then briefly report on the ground segment status in Sect. 5 before concluding.

2. Weak Equivalence Principle

2.1. Weak Equivalence Principle and General Relativity

The Weak Equivalence Principle (aka universality of free fall) states that two bodies in the same gravitational field experience the same acceleration, independently of their mass and composition. Together with the local position invariance (laws of physics do not depend on the position) and the local Lorentz invariance (laws of physics do not depend on the speed of the observer in an inertial frame), this principle constitutes the Einstein Equivalence Principle (EEP), which is at the basis of Einstein's General Relativity. Any violation of the WEP (and of the EEP thereof), would indicate that GR is not the ultimate theory of gravity.

2.2. Tests of the Weak Equivalence Principle

The WEP has been tested throughout the 20th century with an increasing precision (see [6] for a review). Deviations from WEP are usually described by the Eötvös parameter

$$\eta = 2\frac{(m_g/m_i)_A - (m_g/m_i)_B}{(m_g/m_i)_A + (m_g/m_i)_B} \tag{1}$$

where "A" and "B" are two bodies experiencing the same gravitational field, m_g is the gravitational mass and m_i the inertial mass. If the WEP holds, then $m_g = m_i$ for all bodies, and $\eta = 0$. Figure 1 shows how the upper limit on η has decreased during the 20th century, as more accurate experiments have been put forth. The first measurement was made by Eötvös with a torsion pendulum, and allowed him to constrain the WEP at a level of 10^{-8}. Most recently, the monitoring of the Earth and Moon system with the Lunar Laser Range (LLR – e.g. [7, 8]), and the measurement by the Eöt-Wash group with a torsion pendulum, reached the best limits $\eta \leqslant 10^{-13}$ [9]. On-ground measurement are however reaching their limits in terms of signal-to-noise ratio, making a better measurement more difficult. As a consequence, efforts are underway to perform WEP tests with atomic interferometers (e.g. [10]). Another solution to increase the precision on the WEP is to test it in space: this is the goal of the MICROSCOPE mission. Theories currently developed to explain the accelerated expansion of the Universe, or to unify GR and quantum physics, predict that WEP is violated at a level $10^{-18} \leqslant \eta \leqslant 10^{-13}$ [11, 12]. MICROSCOPE is expected to measure η at the level 10^{-15}: it will thus allow us to probe a significant part of the parameter space under consideration by those new theories, and to start discriminating against theories.

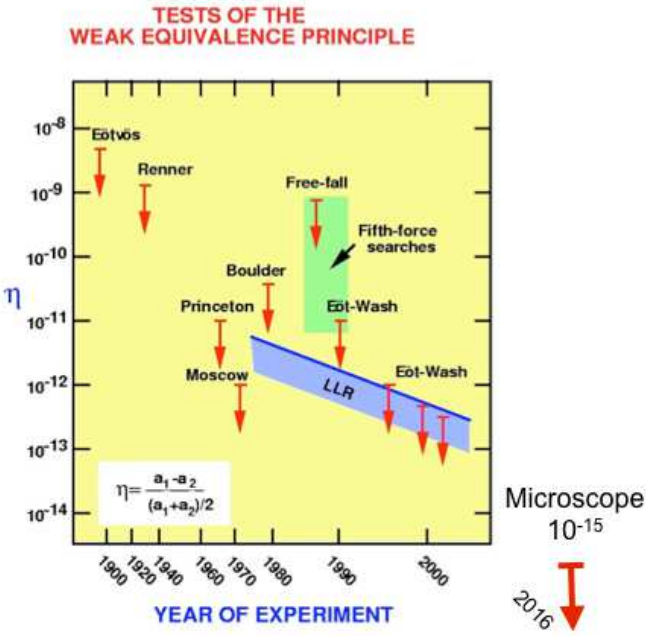

Figure 1. Tests of WEP throughout the 20th century. The arrow on the lower right corner shows the expectation for MICROSCOPE. Figure adapted from [6].

3. MICROSCOPE

MICROSCOPE, launched from Kourou on April 25, 2016, tests the WEP by comparing the acceleration experienced by two free-falling test masses in the Earth's gravity field. To this aim, it embarks two ultrasensitive electrostatic differential accelerometers, each of them consisting of two coaxial cylindrical test masses whose motion is electrostatically constrained.

In one (reference – 'REF') accelerometer, the test masses are made of the same material to demonstrate the experiment's accuracy; they are made of different materials in the second ('EP') accelerometer, which is used to test the WEP. The difference of electric potentials applied to keep the masses in equilibrium is a measure of the difference in the proof masses motion; hence, a non-zero difference of applied potentials is a measure of a WEP violation.

Figure 2 shows the measurement principle for the EP accelerometer. At leading order, its test masses experience the same gravitational field (red arrows) because their centers of mass are very close to each other (of the order of micrometers). In reality, the fact that the centers of mass are not exactly the same lead to a nuisance signal due to the gradient of the Earth's gravity field (see Eq. 2 below), that can easily be corrected for. If the WEP is violated, then the difference in accelerations along the EP test axis (horizontal black arrows, along which the test is performed) will be modulated by the instrument's motion around the Earth. We then expect to detect a sine wave corresponding to the modulation of the difference of the voltages applied in the two test-mass electrostatic configuration to keep them centered. Depending on the spacecraft's spin about the axis normal to the orbital plane (either null for an inertial session as depicted by the figure, or non-null for a spined session), the WEP violation signal will have a typical, expected frequency.

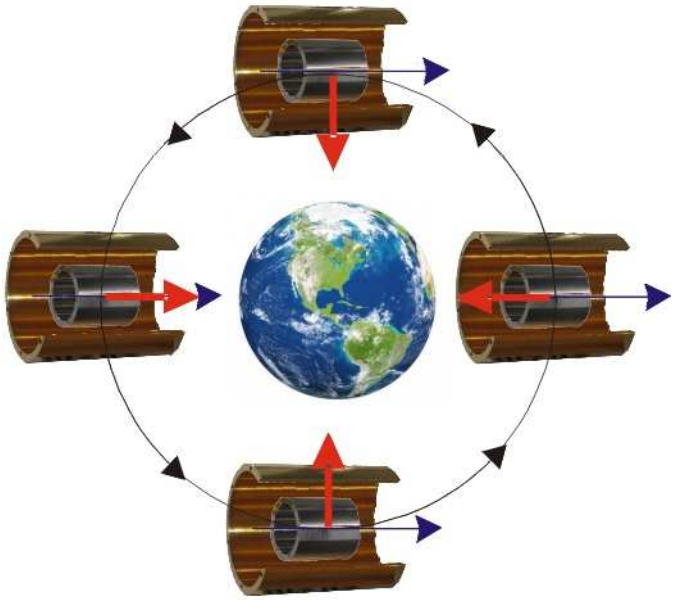

Figure 2. MICROSCOPE's measurement principle.

The difference of acceleration deduced by the measured difference in applied voltages can be written as:

$$\overrightarrow{\Gamma}_{\mathrm{meas,d}} = [\mathcal{M}_c]\left(\eta\overrightarrow{g} + ([\mathcal{T}] - [\mathcal{I}n])\,\overrightarrow{\Delta} - 2\,[\Omega]\dot{\overrightarrow{\Delta}} - \ddot{\overrightarrow{\Delta}}\right) + \overrightarrow{K_{0,d}} + [\mathcal{M}_d]\,\overrightarrow{\Gamma}_{\mathrm{App,c}} + \overrightarrow{\Gamma}_{\mathrm{measquad,d}} + \overrightarrow{\Gamma}_{\mathrm{n,d}} + [\mathcal{C}_d]\,\dot{\overrightarrow{\Omega}} \quad (2)$$

where η is the EP violation signal we are looking for; $\overrightarrow{g}$ is the Earth gravity field at the spacecraft's center-of-mass; $\overrightarrow{\Delta} = \overrightarrow{O_iO_j}$ is the distance between the center of the differential accelerometer's test masses; $\overrightarrow{K}_{0,d}$ is the accelerometer's bias; $[\mathcal{M}_c]$ is the common mode sensitivity matrix; $[\mathcal{T}]$ is the Earth gravity gradient tensor; $[\mathcal{I}n]$ is the inertial acceleration tensor, $[\Omega]\dot{\overrightarrow{\Delta}}$ is the Coriolis acceleration, with $[\Omega]$ the spacecraft's angular velocity matrix;

$[\mathcal{M}_d]$ is the differential mode sensitivity matrix; $\overrightarrow{\Gamma}_{\mathrm{App,c}}$ is the common mode acceleration and includes non-gravitational external accelerations; $\overrightarrow{\Gamma}_{\mathrm{measquad,d}}$ is the quadratic residuals; $\overrightarrow{\Gamma}_{\mathrm{n,d}}$ is the instrument's noise; and $[\mathcal{C}_d]$ is the differential angular to linear coupling matrix. All nuisance parameters are either corrected for through careful modeling (e.g. gravity gradient tensor) or calibrated in flight (e.g. bias [13, 14]), or minimized by design of the instrument and of the satellite (e.g. inertial tensor, instrument's noise).

MICROSCOPE's instrument (T-SAGE – Twin Space Accelerometer for Gravitation Experiment) and its performance have been described elsewhere (e.g. [3, 4]). As aforementioned, the instrument's mechanical core consists of two differential accelerometers (Sensor Units – SU), whose test masses are co-axial cylinders kept in equilibrium with electrostatic actuation. The test masses' materials were chosen carefully so as to maximize the scientific return of the experiment and to optimize their industrial machining: the EP test masses are made of alloys of Platinum-Rhodium (PtRh10 – 90% Pt, 10% Rh) and Titanium-Aluminium-Vanadium (TA6V – 90% Ti, 6% Al, 4% V), while the REF test masses are made of the same PtRh10 alloy. For each SU, the test masses are controlled electrostatically, through electrodes, without any mechanical contact; only a thin 7 μm-diameter gold wire, used to fix the masses' electrical potential to the electronics reference voltage, provides a mechanical contact (and associated, accounted for, damping noise) between the test masses and their cage. The test masses' control is performed by an electronic servo-loop. Two Front End Electronics Unit (FEEU) boxes (one per SU) include the capacitive sensing of masses, the reference voltage sources and the analog electronics to generate the electrical voltages applied to the electrodes; an Interface Control Unit (ICU) includes the digital electronics associated with the servo-loop digital control laws, as well as the interfaces to the satellite's data bus. Additionally, the same electronics' output is used by the drag-free system of the satellite.

Performance analyses predict a noise Amplitude Spectral Density of 10^{-12} m/s^2/Hz$^{1/2}$ in the frequency band $10^{-3} - 0.03$ Hz, compatible with a test of the WEP at a 10^{-15} accuracy (see [3] for a detailed uncertainty analysis).

The spacecraft is derived from the CNES's Myriad series of microsatellites. With a mass of 325 kg and dimensions of 1380x1040x1580 mm^3, it has been designed to be as symmetric as possible, with the T-SAGE instrument sitting at its center-of-mass so that the self-gravity is minimized. No moving mechanical parts can contaminate the Equivalence Principle measurement. Its propulsion system, based on cold gas, is derived from the GAIA mission and supplied by ESA. The MICROSCOPE mission uses a Sun-synchronous, very low eccentricity (1.5×10^{-3}), 710 km orbit.

4. MICROSCOPE's first few months in orbit: commissioning phase status

From early May 2016 to August 2016, the satellite was partially in eclipse. The periodic sun-shade transitions prevented a fine thermal control of the payload, and therefore a robust WEP test. This time was hence dedicated to the satellite's and instrument's commissioning phase. All the modes of the satellite operation were successfully verified. This section presents the status of the satellite and of the mission as of September 2016.

4.1. First in-orbit instrument health checks

The T-SAGE payload was first switched on on May 2nd 2016, one week after launch, after CNES checked orbital parameters and the main satellite's operational functions. The first operation consisted in a health verification in order to assess the integrity of the instrument, while it was still in a pre-launch configuration (i.e. with the test masses blocked in their electrostatic cage). The main functionalities verification were obtained through dedicated housekeeping data as well as through the science data themselves contained in the telemetry:

- at SU level: we checked that the gold wires survived the launch and did not break. The four of them were successfully detected through a specific telecommand. We also checked that all four masses were still blocked.
- at FEEU level: the "as expected" test masses position measurement validated the electronics, the SU/FEEU harness and the SU core integrity.
- at ICU level: we checked that the digital control loop through the open loop response, the data production, the command control, and the power supply were all nominal.

These operations allowed us to confirm the integrity of the instrument, and therefore to go ahead with the mission.

4.2. Test masses release and first control

The early operations' most critical step was the release of the test masses. Its failure would have directly translated into the failure of the mission. Until then, test masses were safely kept motionless by a dedicated mechanical blocking system to prevent any harm during launch. The cylindrical masses were maintained on their top and bottom faces by finger-shaped stops controlled by pressured force actuators. Their release was performed by delivering a specific voltage from the power bus of the satellite, allowing the perforation of the lower stops' valve membrane, therefore allowing the lower stops to get retracted. The instrument was then in its robust mode (also called "acquisition" mode) that delivers sufficient forces to displace the masses. Then, as soon as the blocking fingers were released, the test masses were automatically servo-controlled ("acquired") at the centre of the electrode set. Fig. 3 shows this first release and control of the internal test mass of the EP sensor. Within about 10 seconds and a few oscillations, the mass was brought from its blocked position (75 μm on the sensitive X-axis –blue curve) to the center of the electrostatic cage, where it became controlled electrostically. The four masses were successfully released and electrostatically levitated.

Since then, MICROSCOPE has been providing acceleration and position data for the four test masses' six degrees of freedom. Those data are used for the science output of the mission. The instrument is working and ready to test the Equivalence principle.

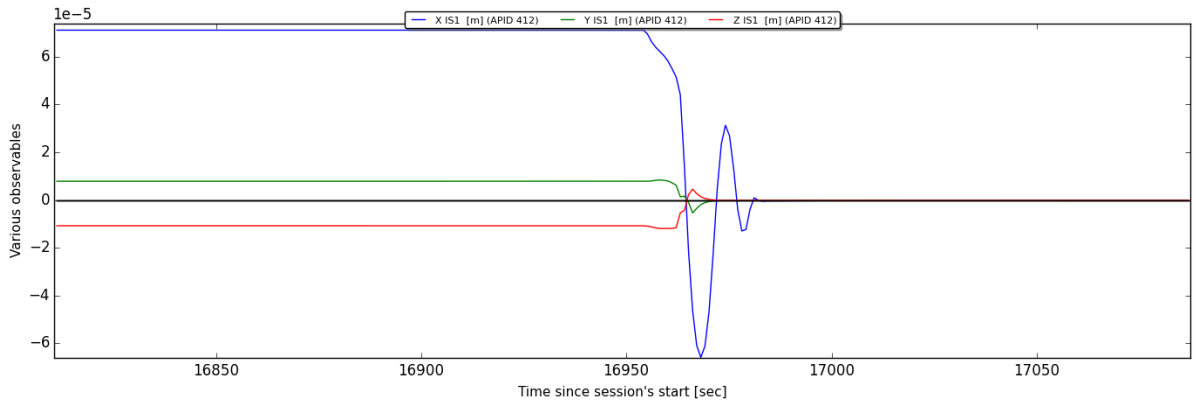

Figure 3. Release of the internal test mass of the EP sensor. The figure shows the position of the mass along its three linear axes (blue: X, green: Y, red: Z), from being blocked to being electrostatically controlled.

4.3. First switch on of the drag-free system

We checked that the simultaneous and continuous drag-free operation on six degrees of freedom is operating correctly. As the drag-free is controlled using a combination of the data provided by the instrument itself and of the satellite's star-tracker, it is a good indication that the instrument works as expected.

Fig. 4 provides 24 hours of data record (from midnight to midnight) during this technical session when the drag free system has been first started. The upper panel shows the acceleration measured along the X-axis, and the lower panel shows the accelerations measured along the Y-axis (blue) and Z-axis (green), as a function of time since midnight. The drag-free control is turned on around t=25000 seconds. Before that, the X-axis acceleration oscillates at the orbital frequency: this oscillation is due to the projection of the atmospheric drag on the X-axis (which lies in the orbital plane). The same behavior can be noticed for the Z-axis (which lies in the orbital plane too, and is therefore also subject to the drag). The Y-axis acceleration does not show any sinusoidal variation (lower panel, blue curve): because the Y-axis is normal to the orbital plane, the acceleration along it is insensitive to the drag. However, we can notice regular dips in the acceleration; they correspond to the satellite passing through the shade (these data have been taking during the eclipse season), when the solar radiation pressure (SRP) disappears. This shows that we can easily measure the SRP. After the drag-free is turned on, those regular patterns disappear, proving that the drag-compensation operates efficiently.

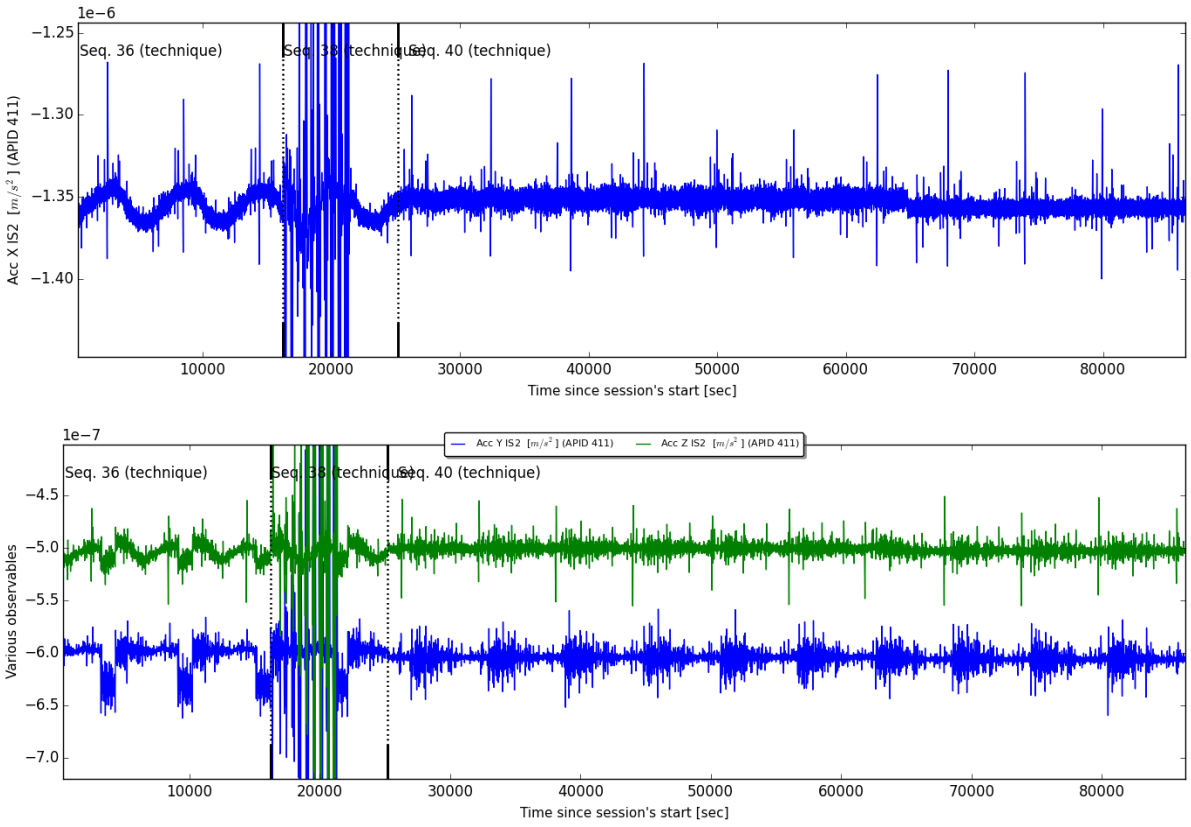

Figure 4. Measured linear accelerations along the X-axis (upper panel) and the Y- and Z-axes (lower panel), around the time the drag compensation was first turned on.

To conclude this section, we can note the periodic pattern of acceleration "bursts" (Fig. 4). Those spikes are due to crackles of the satellite multi-layer insulator, that reacts to the

temperature changes as the satellite goes through the shade area once per orbit, then relaxes. As those spikes may contaminate the WEP test, we developed techniques to correct for them; we discuss them in the next section.

5. Ground Segment, data processing and data analysis status

5.1. Ground segment presentation and status

MICROSCOPE's ground segment operations are centered around three entities: the Command Control Center (CCC) and the Center of Expertise for Compensation of Drag (CECT), hosted by CNES-Toulouse, are in charge of the satellite's operations and drag-free and attitude control respectively, and the Science Mission Center (CMSM), hosted by ONERA-Palaiseau, is in charge of the monitoring and operations of MICROSCOPE's instrument, and of the data processing and analysis. In particular, the CMSM is responsible for (1) ensuring all operational functions to maximize the instrument's operation, (2) day-to-day instrument management and monitoring, (3) weekly mission performance check, (4) proposing modifications of the mission scenario to the Science Working Group, and (5) releasing and archiving the data.

Compatibility tests between CNES and ONERA have been performed in 2015, showing that the ground segment operation were ready. We could check this fact in real life operations since the MICROSCOPE launch; no problem has been found. Data processing and analysis softwares at CMSM are now routinely used to process and monitor the data on a daily basis. We are therefore confident that we can efficiently and immediately analyze the science data.

5.2. Mission scenario

From April 2016 to August 2016, the satellite and all subsystems (in orbit or on ground) have been tested. This acceptance phase was followed by a science acceptance phase until November 2016. During this last phase, calibration and WEP test sessions have been performed with their nominal duration, respectively 5 to 10 orbits and 120 orbits. This phase aims at performing a first guess on performance and at optimizing the procedures, the session's parameters and the ground segment data processes.

For instance, the matching of scale factors for the X axes was performed with less than 2×10^{-4} accuracy. To calibrate this parameter, the output of the drag-free accelerometer is biased by a sine signal at a very well-known frequency. Then the drag-free control system applies a thrust to compensate this stimulus. The accelerometer out of the drag-free loop fills then the sine thrust: the comparison with the initial stimulus at the known frequency gives the ration between the scale factors of the two accelerometers. Thus any common acceleration on the satellite is rejected by this 2×10^{-4} factor once the scale factors are corrected. It is worth noting that the difference of scale factors between the inner and outer tests masses was less than 1.5%, better than the 5% expected. Roughly the same result was obtained on the two SU.

The following step of the mission scenario is quite simple. From November 2016 to May 2017, the next Eclipse period of the year, science sessions should be cumulated in order to reach the best performance thanks to noise reduction with time integration.

5.3. Exorcising the curse of missing data

As mentioned in Sect. 3, a WEP violation signal can be detected as a sine wave corresponding to the modulation of the difference in accelerations experienced by the instrument's test-masses as the satellite orbits the Earth. The main task of the data analysis is therefore to extract this sine wave from the instrumental noise and to estimate its amplitude. Of foremost importance, we expect a small amount of data to be lost (e.g. because of short mechanical crackles –see Sect. 4); as a consequence, the noise will leak from the high frequencies (where its Power Spectral Density –PSD– increases) to the lower frequencies where the WEP violation signal is measured, therefore hampering the signal detection and estimation.

We investigated two ways to deal with missing data when estimating deterministic parameters: (1) accounting for them at the parameter estimation level and (2) fill in missing data before using ordinary parameter estimation techniques.

In Baghi et al. [15], we proposed the KARMA (Kalman-AR Model Analysis) method, a general linear regression method able to deal with incomplete data affected by unknown colored noise. It is based on an autoregressive (AR) fit of the noise that is used to whiten the data through a Kalman filtering process. Hence, the algorithm constructs a good approximation of the best linear unbiased estimator, conditionally to the AR model. This technique accounts for missing data without filling gaps, contrary to those that we present next. However, it does not allow us to visually correct the PSD for the leakage, making the assessment of the noise PSD difficult.

The Modified-Expectation-Condition-Maximization (M-ECM [16]) allows us to use KARMA results to fill in the missing data, and therefore reconstruct the full PSD. In this method, the missing data are efficiently estimated by their conditional expectation as in universal Kriging, based on the circulant approximation of the complete data covariance. After initialization with an autoregessive fit of the noise, a few iterations of estimation/reconstruction steps are performed until convergence of the regression and PSD estimates, in a way similar to the expectation-conditional-maximization algorithm. The estimation can be performed for an arbitrary PSD provided that it is sufficiently smooth.

Another possibility to fill in gaps is to use the inpainting algorithm [17, 18], which reconstructs missing data with a basis functions dictionary using a sparsity prior. We showed that inpainting allows us to recover the noise PSD and to use an ordinary least square method to look for a WEP violation signal.

Conclusion

MICROSCOPE aims to test the Weak Equivalence Principle in space down to an accuracy of 10^{-15}. This is two orders of magnitude better than the current constraints, and will allow us to watch for physics beyond General Relativity. Beside this science goal, MICROSCOPE is fulfilling a technology objective by showing that the technology is ready for extremely fine satellite attitude control and precise drag-free system. This will be of interest for future ambitious missions like eLISA. As of November 2016, the commissioning phase of MICROSCOPE has shown us that MICROSCOPE is on good tracks to complete its objectives.

Acknowledgments

The authors are grateful to the MICROSCOPE mission staff of CNES in Toulouse, the Observatoire de la Côte d'Azur in Grasse and ONERA in Châtillon, for all exchanges about the mission, the satellite, the payload and the science mission center. This work makes use of technical data from the CNES-ESA-ONERA-CNRS-OCA Microscope mission, and has received financial support from ONERA and CNES. JB acknowledges travel financial support from the LISA Symposium organizers, as well as from the UnivEarthS Labex program at Sorbonne Paris Cité (ANR-10-LABX-0023 and ANR-11- IDEX-0005-02)

References

[1] Abbott, B. P., Abbott, R., Abbott, T. D., et al. 2016, Physical Review Letters, 116, 061102
[2] Abbott, B. P., Abbott, R., Abbott, T. D., et al. 2016, Physical Review Letters, 116, 241103
[3] Touboul P. 2009, Space Sci. Rev., 148, 455
[4] Touboul P., Métris G., Lebat V., Robert A. 2012, Classical and Quantum Gravity, 29, 184010
[5] Bergé, J., Touboul, P., & Rodrigues, M., Journal of Physics Conference Series, 610, 012009
[6] Will, C. M. 2006, Living Reviews in Relativity, 9, 3
[7] Murphy, T. W., Jr., Adelberger, E. G., Battat, J. B. R., et al. 2012, Classical and Quantum Gravity, 29, 184005

[8] Williams, J. G., Turyshev, S. G., & Boggs, D. H. 2012, Classical and Quantum Gravity, 29, 184004
[9] Wagner, T. A., Schlamminger, S., Gundlach, J. H., & Adelberger, E. G. 2012, Classical and Quantum Gravity, 29, 184002
[10] Bonnin, A., Zahzam, N., Bidel, Y., & Bresson, A. 2013, Phys. Rev. A, 88, 043615
[11] Damour, T. 2012, Classical and Quantum Gravity, 29, 184001
[12] Overduin, J., Everitt, F., Worden, P., & Mester, J. 2012, Classical and Quantum Gravity, 29, 184012
[13] Hardy, É., Levy, A., Métris, G., Rodrigues, M., & Touboul, P. 2013, Space Sci. Rev., 180, 177
[14] Hardy, É., Levy, A., Rodrigues, M., Touboul, P., & Métris, G. 2013, Advances in Space Research, 52, 1634
[15] Baghi, Q., Métris, G., Bergé, J., et al. 2015, Physical Review D, 91, 062003
[16] Baghi, Q., Métris, G., Bergé, J., et al. 2016, Physical Review D, 93, 122007
[17] Bergé, J., Pires, S., Baghi, Q., Touboul, P., & Métris, G. 2015, Physical Review D, 92, 112006
[18] Pires, S., Bergé, J., Baghi, Q., Touboul, P., & Métris, G. 2016, Physical Review D, 94, 123015